Fig. 3 **a** Dynamic lateral view X-ray images of a 63-year-old female (case 5) indicates osseous integration, 2 years postoperative. **b** Reconstruction CT indicates bony fusion, 2 years postoperative

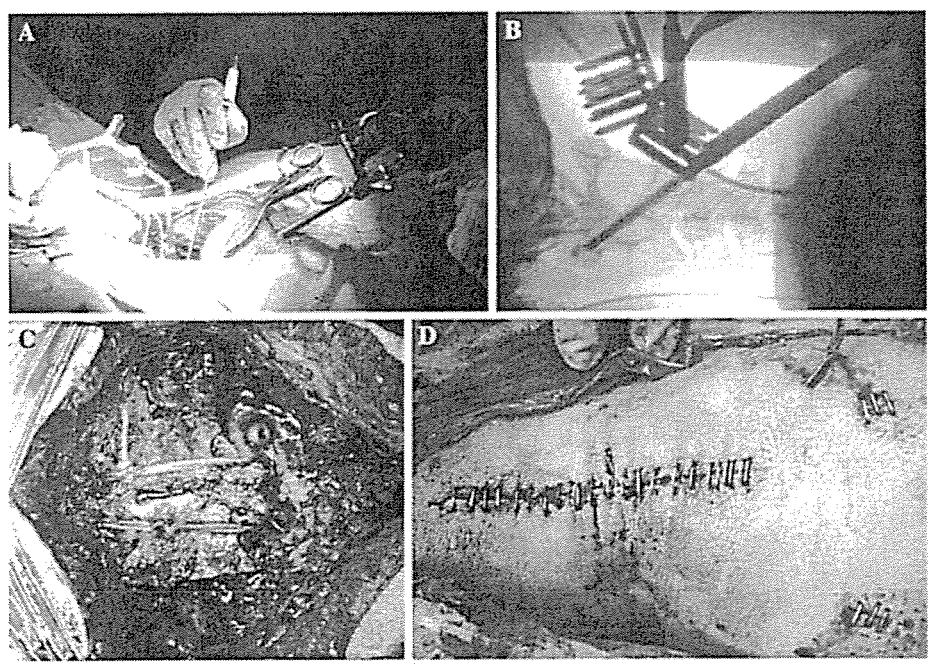

Fig. 4 **a** Case 9: a 54-year-old man during atlanto-axial fixation. The reference frame is placed on the C2 spinous process and a navigatable guide is inserted, in an incision separate from that of the reference frame. **b** Lateral view from image intensifier during surgery. **c** Magerl's and Brooks' procedures were performed using SecureStrand sublaminar cables. **d** Main skin incision and two small incisions

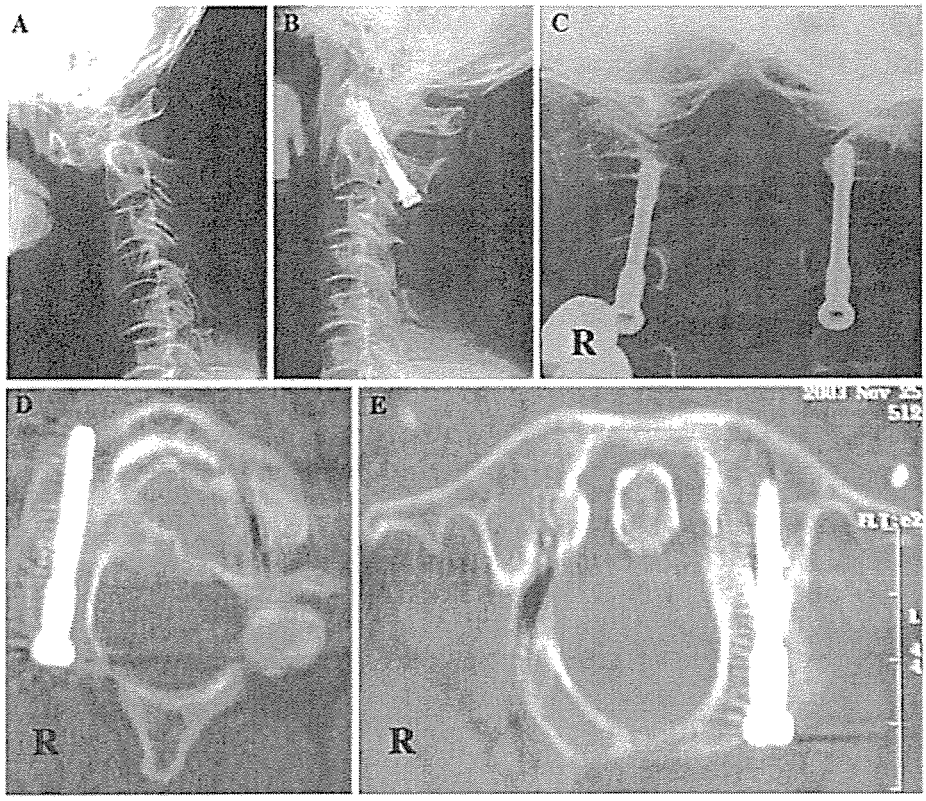

Fig. 5 **a** Preoperative flexion lateral X-ray in case 9 indicates atlanto-axial subluxation. **b** Postoperative lateral X-ray. **c** Postoperative antero-posterior X-ray. **d** & **e** Postoperative reconstructive CT shows transarticular screws correctly passing through the pedicle of C2 and C1/2 joints

authors judged that it was not possible to insert the pedicle screw into the C2, C4, and, C5 (hemilateral) pedicles. The following procedures were performed using the navigation system: C1 laminectomy, insertion of bilateral C3 and hemi lateral C5 pedicle screw (RRS Loop Spinal System; Robert Leid, Tokyo, Japan), sublaminar cable fixation from C2 to C5 (using SecureStrand sublaminar cables), and insertion of occipital screw. Posterior bone graft from C0 to C5 was performed after instrumentation. Neurological deficits and occipital pain had resolved, and surgery enabled the patient to walk again. The postoperative CT scan (C3 level) shows accurate placement of the pedicle screws, which were inserted into extremely narrow pedicles (Fig. 6). After 48 months post-surgery, the patients showed improvement from 3B (preoperatively) to 3A according to Ranawat's classification.

Discussion

Cervical reconstruction surgery should be considered to maintain the quality of life and daily activities in RA patients with severe cervical involvements. A recent study indicated that the natural course of RA patients with myelopathy managed by conservative treatments is poor [25]. In their study, all patients did not recover and were bedridden. Furthermore, all patients had died within 3 years [25]. Casey [5] reported that no benefit was obtained except pain relief by surgical treatment of patients of Ranawat's class 3B. In contrast, the current study showed the potential importance of surgery for class 3B patients, which provided excellent clinical results.

One of the main goals of cervical reconstruction surgery in RA patients is to eliminate instability by achieving immediate and long-term stability. Pedicle screw fixation and C1/2 transarticular screw fixation are biomechanically superior to other conventional procedures using wiring or clamping [1, 9, 14, 17]. Furthermore, pedicle screw fixation is a useful technique because laminectomy or laminoplasty can be performed simultaneously.

Conventional screw insertion techniques for both C1/2 screw and pedicle screw placement in the subaxial cervical spine rely on anatomical landmarks and intraoperative fluoroscopy. However, in RA patients, several specific illness-related problems of the cervical spine make surgical treatment extremely difficult. The use of corticosteroid medication for several years and immobilization of the spine caused by multiple musculoskeletal deformities and dysfunctions lead to

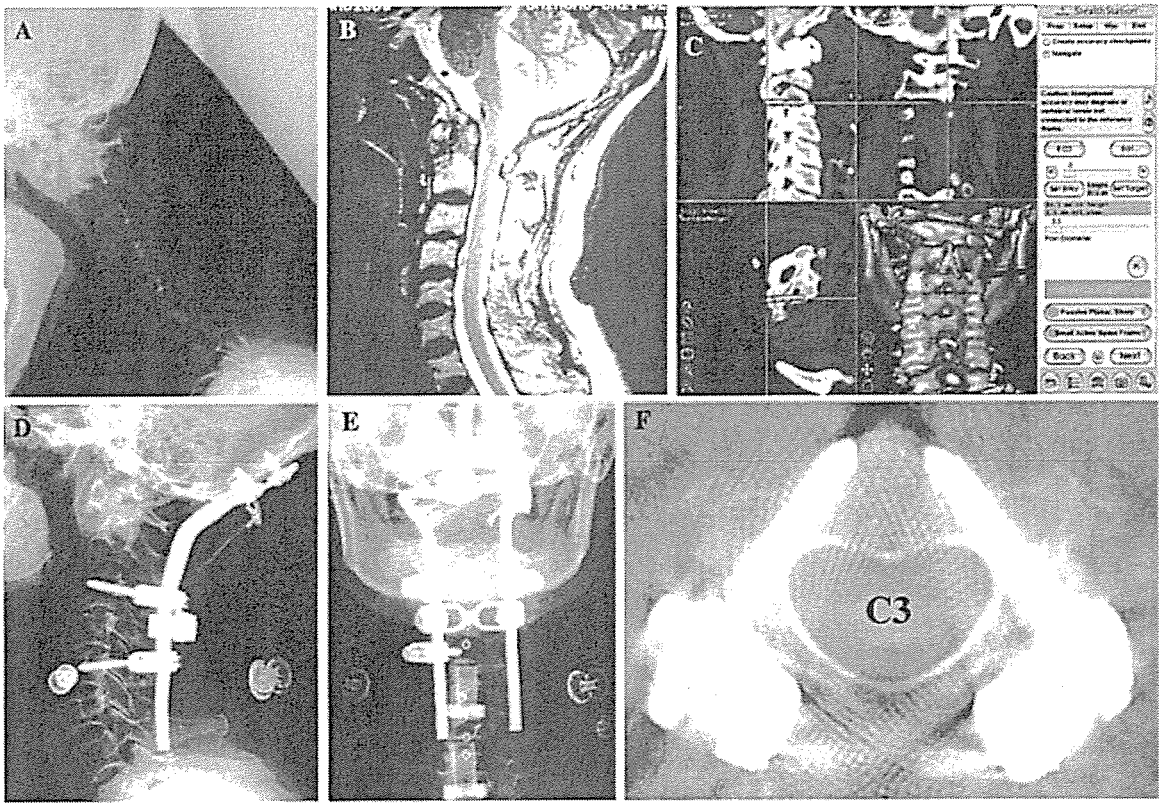

Fig. 6 **a** Preoperative flexion lateral X-ray in a 62-year-old female (case 10) indicates atlanto-axial subluxation and vertical subluxation. **b** Preoperative sagittal T2-WI MRI shows cord compression due to C1 laminae. **c** Computer display shown at surgery. **d, e** Postoperative X-ray. **f** Postoperative CT scan (C3 level) shows pedicle screw was inserted accurately

considerable osteoporosis. Moreover, due to erosion of the anatomical structures, bony landmarks are not always reliable. Especially when the vertebral artery runs an abnormal course, screw placement has a potential risk of neurovascular injury, and vertebral artery injury on the dominant side can cause cerebellar infarction and possibly fetal sequelae [2, 22, 23]. Moreover, due to severe spinal deformity and small anatomical size of the vertebra (the lateral mass and pedicle) in the most RA cervical lesions, screw placement procedures are highly technically demanding and pose the potential risk of neurovascular injuries even though intraoperative fluoroscopy is used. The current study clearly shows from clinical results that computer-assisted screw insertion in the rheumatoid cervical spine enables a significant reduction in the screw malplacement rates (1/48; 2.1%) as compared to conventional insertion techniques, using image intensifier (5.3%; Abumi K et al. [1]). There are currently no published reports on perforation rates with cervical pedicle screws in rheumatoid cervical spine lesions. All procedures performed at this facility were performed using a navigation system, therefore no control data is available. Borm et al. [4] reported that transarticular C1–C2 screw fixation was performed in 14 cases using computer navigation (STN 4.0; Zeiss Company, Oberkochen Germany). In this study, there was one medial perforation of a C2 pedicle wall and one malposition of the screw in C2 without reaching the lateral mass of C1 (2/28; 7.1%). In contrast, there were no malpositions of the transarticular C1–C2 screw fixation among our cases. Regarding C1-2 transarticular screw fixation, it is very easy to navigate at C2 levels using image-guidance systems. However, C1 is easily moved in the prone position even if a Halo-vest apparatus is adapted for patients with atlantoaxial subluxation. In such a case, it is difficult to navigate the screw in the lateral mass of the atlas, and a two-dimensional image intensifier during surgery should be employed. However, this type of image intensifier was not used in pedicle screw insertion in this study. When pedicle perforation was suspected, it was investigated on X-ray image using a marker. Importantly, although the risk of screw perforation can be reduced using a navigation system, its incidence does not disappear completely. Due to the fragile bone quality of the RA cervical

spine, care must be taken during rod or plate application procedures and reduction maneuvers which may cause cut-out and displacement of the screw from its original position. To prevent these injuries, preoperative evaluation of the vertebral artery and planning of screw insertion are indispensable. Generally, insertion of screws into the pedicle of less than 3.5 mm in diameter should be avoided even with navigation assistance.

Preoperative vertebral artery evaluation by MR angiography revealed unilateral stenosis or occlusion in 23.8% of patients, all of whom were complicated with VS. Abnormality of vertebral artery is highly likely in RA patients because of cervical deformity. Tumialan et al. [26] reported cerebral and cerebellar infarction in rheumatoid cervical spine patients caused by vertebral artery injury, observed during anterior corpectomy. In consideration of that report, in case of vertebral artery occlusion or stenosis, no pedicle screws were used on the artery-dominant side to avoid vertebrobasilar ischaemia and concurrent stroke if pedicle diameter was narrow. This approach shows significant benefits of preoperative planning using the navigation system.

The accuracy of a computer-assisted image-guidance system for correct pedicle screw fixation of the cervical spine has been confirmed in laboratory tests [12], but its clinical results in RA patients have not been clarified. Although the current study was not large in number of patients, the results of surgery under the image-guidance system were encouraging. Use of this system in cervical instrumentation surgery for RA patients can aid in reducing the risk of screw misplacement.

Conclusion

In this study, the authors demonstrated that image-guidance systems can be applied safely to the cervical lesions caused by RA. Image-guidance systems are useful tools in preoperative planning and in transpedicular screw placement in the cervical spine of RA patients. However, incidence of screw perforation does not disappear completely. Due to the fragile bone quality of RA cervical spine, care must be taken during rod or plate application procedures and reduction maneuvers.

References

1. Abumi K, Kaneda K, Shono Y, Fujiya M (1999) One-stage posterior decompression and reconstruction of the cervical spine by using pedicle screw fixation systems. J Neurosurg (Spine 1) 90:19–26
2. Abumi K, Shono Y, Ito M, Taneichi H, Kotani Y, Kaneda K (2000) Complications of pedicle screw fixation in reconstructive surgery of the cervical spine. Spine 25:962–969
3. Amiot LP, Labelle H, DeGuise JA, Sati M, Brodeur P, Rivard CH (1995) Computer-assist pedicle screw fixation. A feasibility study Spine 20:1208–1212
4. Borm W, Konig RW, Albrecht A, Richter HP, Kast E (2004) Percutaneous transarticular atlantaxial screw fixation using a cannulated screw system and image guidance. Minim Invasive Neurosurg 47:111–114
5. Casey ATH, Crockard HA, Bland JM, Stevens J, Moskovich R, Ransford AO (1996) Surgery on the rheumatoid cervical spine for the non-ambulant myelopathic patients-too much, too late? Lancet 347:1004–1007
6. Clark CR (1994) Rheumatoid involvement of the cervical spine. An overview. Spine 19:2257–2258
7. Fuji T, Oda T, Kato Y, Fujita S, Tanaka M (2000) Accuracy of atlantoaxial transarticular screw insertion. Spine 25: 1760–1764
8. Golfinos JG, Fitzpatrick BC, Smith LR, Spetzler RF (1995) Clinical use of a flameless stereotactic arm: results of 325 cases. J Neurosurg 83:197–205
9. Grob D, Crisco JJ 3rd, Panjabi MM, Wang P, Dvorak J (1992) Biomechanical evaluation of four different posterior atrantoaxial fixation techniques. Spine 17:480–490
10. Jones EL, Heller JG, Silcox DH, Hutton WC (1997) Cervical pedicle screws versus lateral mass screws. Anatomic feasibility and biomechanical comparison. Spine 22:977–982
11. Kamimura M, Ebara S, Itoh H, Tateiwa Y, Kinoshita T, Takaoka K (1999) Accurate pedicle screw insertion under control using a computer-assisted image guiding system: laboratory test and clinical study. J Orthop Sci 4:197–206
12. Kamimura M, Ebara S, Itoh H, Tateiwa Y, Kinoshita T, Takaoka K (2000) Safe and accurate cervical pedicle screw insertion guided by a computer assisted image-guidance system. J Spinal Disord 13:218–225
13. Kast E, Mohr K, Richter HP, Borm W (2006) Complication of transpedicular screw fixation in the cervical spine. Eur Spine J 15:327–334
14. Kotani Y, Cunningham BW, Abumi K, McAfee PC (1994) Biomechanical analysis of cervical stabilization systems: an assessment of transpedicular screw fixation in the cervical spine. Spine 17:2529–2539
15. Laine T, Lund T, Ylikoski M, Lohikoski J, Schlenzka D (2000) Accuracy of pedicle screw insertion with and without computer assistance: a randomized controlled clinical study in 100 consecutive patients. Eur Spine J 9:234–240
16. Madawi AA, Casey AT, Solanki GA, Tuite G, Veres R, Crockard HA (1997) Radiological and anatomical evaluation of the atrantoaxial transarticular screw fixation technique. J Neurosurg 86:961–968
17. Magerl F, Seemann PS (1987) Stable posterior fusion of the atlas and axis by transarticular screw fixation. In: Kehr P, Weidner A (eds) Cervical spine I. Springer, Berlin Heidelberg New York, pp 322–327
18. Nolte LP, Zamorano LJ, Jiang Z, Wang Q, Langlotz F, Berlemann U (1995) Image-guided insertion of transpedicular screws. A laboratory set-up. Spine 20:497–500
19. Ranawat CS, O'Leary P, Pellici P (1979) Cervical spine fusion in rheumatoid arthritis. J Bone Joint Surg 61A: 1003–1010
20. Santavirta S, Konttinen Y, Laasonen E, Honkanen V, Antti-Poika I, Kauppi M (1991) Ten-year results of operations for rheumatoid cervical spine disorders. J Bone Joint Surg 73B:116–120

21. Sharp J, Purser DW, Lawrence JS (1958) Rheumatoid arthritis of the cervical spine in the adult. Ann Rheum Dis 17:303–313
22. Shintani A, Zervas NT (1972) Consequence of ligation of the vertebral artery. J Neurosurg 36:447–450
23. Smith MD, Emery SE, Dudley A, Murray KJ, Leventhal M (1993) Vertebral artery injury during anterior decompression of the cervical spine. A retrospective review of ten patients. J Bone Joint Surg 75B:410–415
24. Sumi M, Kataoka O, Ikeda M, Sawamura S, Uno K, Siba R (1997) Atlantoaxial dislocation: a follow-up study of surgical results. Spine 22:759–764
25. Sunahara N, Matsunaga S, Mori T, Ijiri K, Sakou T (1997) Clinical course of conservatively managed rheumatoid arthritis patients with myelopathy. Spine 22:2603–2608
26. Tumialan LM, Wippold FJ 2nd, Morgan RA (2004) Tortuous vertebral artery injury complicating anterior cervical spinal fusion in a symptomatic rheumatoid cervical spine. Spine 29:E343–E348
27. Wright NM, Lauryssen C (1998) Vertebral artery injury in C1–2 transarticular screw fixation: results of a survey of the AANS/CNS Association of Neurological Surgeon/Congress of Neurological Surgeons. J Neurosurg 88:634–640

In Vivo Three-Dimensional Kinematics of the Midcarpal Joint of the Wrist

Hisao Moritomo, Tsuyoshi Murase, Akira Goto, Kunihiro Oka, Kazuomi Sugamoto and Hideki Yoshikawa
J. Bone Joint Surg. Am. 88:611-621, 2006. doi:10.2106/JBJS.D.02885

IN VIVO THREE-DIMENSIONAL KINEMATICS OF THE MIDCARPAL JOINT OF THE WRIST

BY HISAO MORITOMO, MD, TSUYOSHI MURASE, MD, AKIRA GOTO, MD, KUNIHIRO OKA, MD, KAZUOMI SUGAMOTO, MD, AND HIDEKI YOSHIKAWA, MD, PHD

Investigation performed at the Department of Orthopaedic Surgery, Osaka University, Osaka, Japan

Background: The human carpus is a complex joint system. Many problems that arise in the wrist are the result of an alteration of intercarpal motion. Although the midcarpal joint is a major component of the wrist joint, the global kinematics of the midcarpal joint have not been described. The purpose of this study was to provide a simplified description of the motion and function of the midcarpal joint.

Methods: We studied the in vivo three-dimensional kinematics of the midcarpal joint with use of a markerless bone-registration technique. Magnetic resonance images of the wrists of twenty-four healthy volunteers were acquired during a dart-throwing motion or flexion-extension motion of the wrist. Three-dimensional animations of the isolated midcarpal joint were created. Relative midcarpal motions were investigated qualitatively and quantitatively.

Results: The direction of the capitate motion relative to the scaphoid was always similar: it was oblique and it extended from radiodorsal to ulnopalmar in radioulnar deviation, in the dart-throwing motion, and in the flexion-extension motion. The directions of the capitate motions relative to the lunate and triquetrum inclined in a similar way, while the ranges of motion were almost unchanged. As the wrist motion changed from radioulnar deviation to flexion-extension motion, the range of the capitate rotation relative to the scaphoid decreased while the range of the lunate rotation relative to the scaphoid increased. Regardless of the type of wrist motion, the loci of the displacement of all of the joint surfaces of the midcarpal joint were located within a midcarpal ovoid space, and a line connecting the centers of the joint surfaces of the midcarpal joint could be schematized as a letter "C" entwining the midcarpal ovoid.

Conclusions: Midcarpal motion is essentially the combined motion of three types of joint systems: (1) the uniaxial joint between the scaphoid and the distal row; (2) the biaxial joint between the lunate and triquetrum and the distal row; and (3) the intercarpal joints of the proximal row, which have an adaptive mechanism that accommodates the above-mentioned two types of joint systems in the midcarpal joint.

Clinical Relevance: We advocate use of the "ovoid/C" concept to describe the function of the midcarpal joint that contributes to both the stability and the mobility of the wrist, to assist clinicians in achieving a better understanding of the kinematics of the wrist joint.

The human carpus is a complex joint system interposed between the forearm and the hand. Knowledge of intercarpal kinematics should be of value both from a basic-science perspective and from a clinical point of view because many problems that arise in the wrist are the result of an alteration of intercarpal motion[1]. There is little relative motion between the four bones of the distal row (the trapezium, trapezoid, capitate, and hamate)[2-4], whereas there is greater relative motion between the three bones of the proximal row (the scaphoid, lunate, and triquetrum)[3,5,6]. Although the midcarpal joint is a major component of the wrist joint, the global kinematics of this joint have not been described, to our knowledge.

In a previous study[7], we investigated the kinematics of the midcarpal joint during radioulnar deviation of the wrist and found that the midcarpal motion is more synchronous than had been previously reported. The axes of the rotations of the capitate relative to the scaphoid, lunate, and triquetrum during radioulnar deviation were found to be located closely in space. The isolated midcarpal motions during radioulnar deviation were found to be rotations in the dart-throwing plane of the wrist, extending from radiodorsal to ulnopalmar.

The current study is a continuation of the previous investigation of radioulnar deviation[7]; it was designed to examine midcarpal kinematics during the dart-throwing motion and flexion-extension motion of the wrist and to compare them with midcarpal kinematics during radioulnar deviation.

The purpose of this study was to provide a simplified description of the motion and function of the midcarpal joint.

Materials and Methods

The in vivo three-dimensional kinematics of the midcarpal joint in the right wrists of twenty-four healthy volunteers was studied with a markerless bone-registration technique. We separately investigated the kinematics during the dart-throwing motion in twelve volunteers and the kinematics during the flexion-extension motion in the other twelve. The average age was twenty-six years (range, twenty to thirty-two years) for the volunteers included in the analysis of the dart-throwing motion and twenty-five years (range, twenty to thirty-two years) for those included in the analysis of the flexion-extension motion. Nine men and three women participated in the study of the dart-throwing motion, and eight men and four women participated in the study of the flexion-extension motion. All volunteers consented to be included in the study.

Magnetic resonance images were acquired with the same method as was used in our previous studies[7,8]. To immobilize the elbow and the wrist at a specific angle during the dart-throwing and flexion-extension motions, a special posture device with a grip bar and goniometers was used[9]. This device has three motion axes, which all cross perpendicularly at the wrist joint and enable the wrist to move along any specific plane.

For five of the twelve wrists in the group performing the dart-throwing motion, magnetic resonance images were acquired in six positions from 60° of radial deviation/extension to 40° of ulnar deviation/flexion in 20° increments in the dart-throwing plane. For five of the twelve wrists in the group performing the flexion-extension motion, magnetic resonance images were acquired in seven positions from 60° of extension to 60° of flexion in 20° increments in the sagittal plane. For the other seven patients in each group, magnetic resonance images were acquired in three positions (a neutral position and two extreme positions). We set the dart-throwing motion as an oblique wrist motion relative to the sagittal plane of the wrist in an attempt to reproduce the motion of the throwing of a dart or the hammering of a nail.

The contours of each bone were mapped from magnetic resonance volume images, and three-dimensional surface models of the bones were constructed with use of a software program (Virtual Place-M; Aze, Tokyo, Japan)[7]. The kinematic variables were calculated by registering the bone in one position and comparing it with another. The volume registration technique employed in this study was performed with use of the same software program.

The radius and all of the carpal bones except the pisiform were registered, and the relative motion of each bone was calculated. Three-dimensional animations of the relative motions were created by gradually rotating bones around their own axis of rotation between two adjacent positions and connecting them with use of originally developed software (Orthopedics Viewer; Osaka University, Osaka, Japan). We created animations of all twenty-four wrists and compared the animations of the ten wrists subjected to incremental motion analysis with the animations of the fourteen wrists that were studied in only three positions. We observed a marked similarity between them; thus, we calculated the kinematic variables from the combined data of all wrists.

The coordinate system was constructed with use of osseous landmarks with the wrist in neutral position. The z axis (the supination-pronation axis) was defined as the long axis of the distal part of the radius. The x axis (the flexion-extension axis) was defined as a line passing through the center of the capitate body at a right angle to the z axis and parallel to a line connecting the radial and ulnar styloids. The y axis (radioulnar deviation axis) was defined as a line perpendicular to the other two axes. In our definition of the anatomical planes, we considered the sagittal plane to equal the flexion-extension plane, the coronal plane to equal the radioulnar deviation plane, and the axial plane to equal the supination-pronation plane.

Direction of Global Wrist Motion

The direction of global wrist motion was defined as a line connecting two centroids of the capitate at the two extreme wrist positions on the basis of the assumption that there is little motion between the third metacarpal and the capitate[10]. The angle between the direction of global wrist motion and the x axis of the coordinate system was calculated as viewed in the axial plane.

Midcarpal Motion

Midcarpal motion was investigated by assessing capitate motion relative to the scaphoid, lunate, and triquetrum as well as by analyzing scaphoid, lunate, and triquetrum motions relative to the capitate. If the capitate is used as a reference to determine the kinematics of the proximal row, one can observe all of the relative motions in the midcarpal joint at the same time because there is very little motion between the four bones of the distal row[2-4]. The axes of rotations[11] between the two extreme positions of the capitate relative to the scaphoid, lunate, and triquetrum were the only ones calculated. The range of motion of the capitate was calculated as an angle of rotation around each axis of rotation.

Motion Between the Scaphoid and Lunate and Between the Lunate and Triquetrum

The ranges of motion of the scaphoid and triquetrum relative to the lunate were also calculated as an angle of rotation around each axis of rotation relative to the lunate. The angle was defined as positive when the scaphoid or triquetrum rotated palmarly relative to the lunate in the wrist motion from radial deviation/extension to ulnar deviation/flexion or from extension to flexion.

Relationship Between the Midcarpal Kinematics and the Radiocarpal Kinematics

To compare the midcarpal kinematics with the radiocarpal kinematics, the axes of rotations of the scaphoid and lunate relative to the radius were also investigated. Relationships between the axes of rotations of the midcarpal and radiocarpal joints were analyzed by comparing the location of the axes of rota-

tions of the radiocarpal joint with the primary axis of rotation of the midcarpal joint at the neutral position of the wrist.

Statistical Analysis

All data were expressed as the mean and standard deviation. Statistical analysis of differences was performed with use of the Student t test, with $p < 0.05$ considered to be significant.

Results

Direction of Global Wrist Motion

The angles between the direction of the global wrist motion and the wrist flexion-extension axis in the axial plane were 59° ± 9° in the dart-throwing motion and 91° ± 8° in the flexion-extension motion. Of the twelve wrists studied in flexion-extension motion, four showed an angle of <90° (mean, 82° ± 4°;

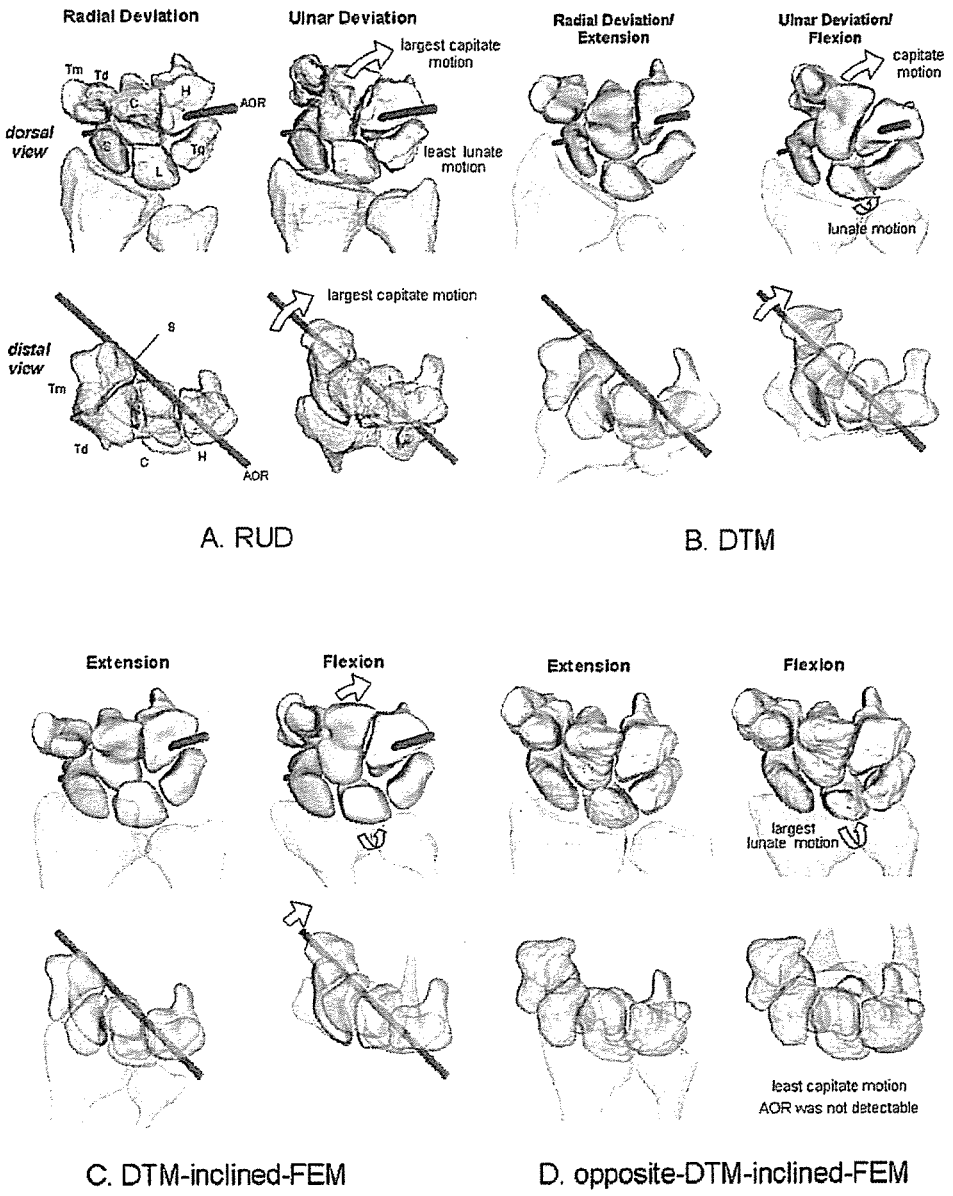

Fig. 1

Dorsal and distal views of the scaphoid-based motions of the right wrist and the axes of rotation (AOR) of the capitate relative to the scaphoid. *A:* Radioulnar deviation (RUD). *B:* Dart-throwing motion (DTM). *C:* Dart-throwing-motion-inclined flexion-extension motion (FEM), and *D:* opposite-dart-throwing-motion-inclined flexion-extension motion. The amount of motion is related to the length of the arrows. S = scaphoid, L = lunate, Tq = triquetrum, Tm = trapezium, Td = trapezoid, C = capitate, and H = hamate. (See Appendix for accompanying video.)

TABLE 1 Kinematic Data During Dart-Throwing Motion

			Angle to Axis for Wrist Flexion and Extension *(deg)*					
Case	Age *(yr)*	Gender	Direction of Global Wrist Motion	Axis of Rotation of Capitate to Scaphoid	Axis of Rotation of Capitate to Lunate	Axis of Rotation of Capitate to Triquetrum	Axis of Rotation of Scaphoid to Radius	Axis of Rotation of Lunate to Radius
1	26	M	55	33	23	21	20	68
2	30	M	56	45	38	35	49	81
3	27	M	57	61	32	43	14	18
4	25	F	58	32	20	21	2	8
5	30	M	69	29	20	6	32	54
6	24	M	69	37	26	27	6	13
7	32	M	66	35	17	17	21	32
8	25	M	73	33	13	14	3	20
9	32	M	43	23	6	12	36	65
10	21	F	47	37	36	24	59	80
11	25	M	56	42	18	8	24	63
12	20	F	62	48	35	13	8	24
Average			59	38	23	20	23	44
Stand. dev.			9	10	10	11	18	27

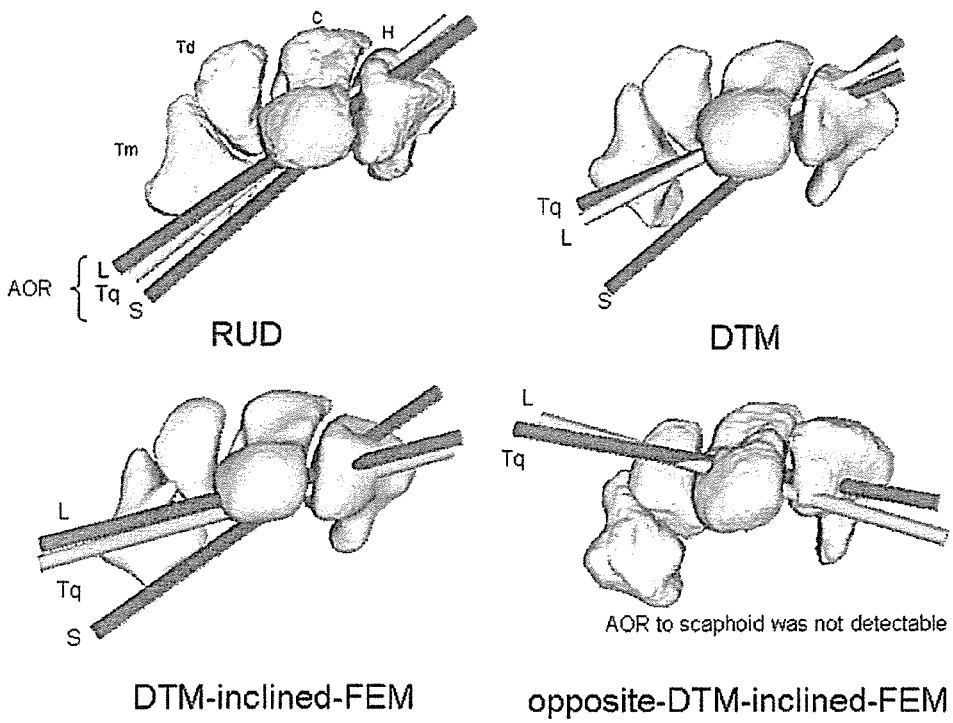

Fig. 2

Proximal view of the distal row of the right wrist and the axes of rotation (AOR) of the capitate relative to the scaphoid (S), lunate (L), and triquetrum (Tq) during radioulnar deviation (RUD), the dart-throwing motion (DTM), the dart-throwing-motion-inclined flexion-extension motion (FEM), and opposite-dart-throwing-motion-inclined flexion-extension motion. Tm = trapezium, Td = trapezoid, C = capitate, and H = hamate.

TABLE 1 *(continued)*

Range of Motion Around Axis of Rotation *(deg)*						
Capitate to Scaphoid	Capitate to Lunate	Capitate to Triquetrum	Scaphoid to Lunate	Triquetrum to Lunate	Scaphoid to Radius	Lunate to Radius
59	76	60	20	19	26	12
37	48	40	12	11	28	20
29	35	27	15	9	65	51
27	74	66	47	8	75	27
30	46	30	17	18	33	25
31	40	33	11	8	26	15
40	44	44	18	11	37	30
39	66	55	32	11	54	27
42	67	53	30	15	63	38
28	37	37	9	9	19	11
35	61	46	32	18	47	25
50	58	41	14	26	33	21
37	54	44	21	14	42	25
10	14	12	11	6	18	11

range, 78° to 87°), which means that the plane of global wrist motion inclined slightly toward a dart-throwing-motion plane (the dart-throwing-motion-inclined flexion-extension-motion group). The other eight wrists showed an angle of >90° (mean, 96° ± 4°; range, 91° to 103°), which means that the plane of global wrist motion inclined slightly toward an opposite-dart-throwing-motion plane (the opposite-dart-throwing-motion-inclined flexion-extension-motion group).

Midcarpal Motion

Motion of the Distal Row Relative to the Scaphoid

The scaphoid-based animation showed the direction of capitate motion relative to the scaphoid to be always similar: it was oblique and it extended from radiodorsal to ulnopalmar in radioulnar deviation, in the dart-throwing motion, and in the dart-throwing-motion-inclined flexion-extension motion. From wrist radial deviation, radial deviation/extension, or extension to wrist ulnar deviation, ulnar deviation/flexion, or flexion, respectively, the capitate always moved from radiodorsal to ulnopalmar (Fig. 1, *A*, *B*, and *C*; see Appendix for videos).

The axes of rotation between the scaphoid and capitate in radioulnar deviation, in the dart-throwing motion, and in the dart-throwing-motion-inclined flexion-extension motion were located closely in space and obliquely penetrated the neck of the capitate from a radiopalmar to an ulnodorsal direction. In the axial plane, the axes of rotation of the capitate relative to the scaphoid in radioulnar deviation, in the dart-throwing motion, and in the dart-throwing-motion-inclined flexion-extension motion formed a radially and palmarly opening angle of 43° ± 7° (as previously reported[7]), 38° ± 10°, and 31° ± 9°, respectively, with the wrist flexion-extension axis (Tables I and II). There were no significant differences between these angles.

In the opposite-dart-throwing-motion-inclined flexion-extension motion, the capitate seldom moved and the scaphotrapeziotrapezoid joint appeared to be "locked" (Fig. 1, *D*; see Appendix for videos). The axes of rotation between the scaphoid and capitate in the opposite-dart-throwing-motion-inclined flexion-extension motion varied considerably (mean angle with the wrist flexion-extension axis, 5° ± 53°) so that a consistent pattern of the axis of rotation was not detectable. In some wrists (Cases 20 and 24), the intercarpal joints between the trapezium, trapezoid, and capitate showed irregular motions; the trapezium and trapezoid translated distalward relative to the trapezoid and capitate, respectively, when the wrist moved from extension to flexion.

As the global wrist motion changed from radioulnar deviation to the opposite-dart-throwing-motion-inclined flexion-extension motion, the range of the capitate rotation relative to the scaphoid gradually decreased. The ranges of rotation of the capitates around their own axes of rotation were 41° ± 10° in radioulnar deviation (as previously reported[7]), 37° ± 10° in the dart-throwing motion, 27° ± 5° in the dart-throwing-motion-inclined flexion-extension motion, and 9° ± 15° in the opposite-dart-throwing-motion-inclined flexion-extension motion (Tables I and II). There were significant differences between the values in radioulnar deviation and the dart-throwing-motion-inclined flexion-extension motion ($p < 0.05$), between those in the dart-throwing motion and the dart-throwing-motion-inclined flexion-extension motion ($p < 0.05$), and between those in the dart-throwing-motion-inclined

TABLE II Kinematic Data During Flexion-Extension Motion

Wrist Motion/Case	Age (yr)	Gender	Angle to Axis for Wrist Flexion and Extension (deg)					
			Direction of Global Wrist Motion	Axis of Rotation of Capitate to Scaphoid	Axis of Rotation of Capitate to Lunate	Axis of Rotation of Capitate to Triquetrum	Axis of Rotation of Scaphoid to Radius	Axis of Rotation of Lunate to Radius
Dart-throwing-motion-inclined flexion-extension motion								
13	30	M	78	21	18	11	6	5
14	24	M	80	40	16	18	1	−3
15	27	M	87	25	2	0	−8	1
16	24	F	84	38	17	28	−2	−1
Average			82	31	13	14	−1	1
Stand. dev.			4	9	7	12	6	3
Opposite-dart-throwing-motion-inclined flexion-extension motion								
17	25	F	92	−14	−1	−13	8	12
18	26	M	95	−25	−15	3	0	1
19	30	M	99	−54	−19	−20	−5	−12
20	24	M	103	87	−59	−31	−8	2
21	32	M	91	−2	−3	0	0	0
22	20	F	92	−48	−16	−22	−8	−8
23	21	F	96	16	−12	−22	−2	−5
24	25	M	98	78	−22	−24	0	−2
Average			96	5	−18	−16	−2	−2
Stand. dev.			4	53	18	12	5	7
Total average			91	14	−8	−6	−2	−1
Stand. dev. for total average			8	45	21	19	5	6

flexion-extension motion and the opposite-dart-throwing-motion-inclined flexion-extension motion ($p < 0.05$).

Motion of the Distal Row Relative to the Lunate and Triquetrum

When the global wrist motion changed from radioulnar deviation to the opposite-dart-throwing-motion flexion-extension motion, the directions of the capitate motions relative to the lunate and triquetrum inclined in a similar way, which was clearly different from the capitate motion relative to the scaphoid. The capitate motions relative to the lunate and triquetrum in the midcarpal joint were essentially similar and synchronous with each other regardless of the type of wrist motion.

The axes of rotation of the capitate relative to the lunate and triquetrum in the dart-throwing motion and flexion-extension motion ran more transversely in the axial plane than did those during radioulnar deviation (Fig. 2). The axes of rotation of the capitate relative to the lunate and triquetrum formed, with the wrist flexion-extension axis, a radially and palmarly opening angle of 41° ± 11° and 42° ± 14°, respectively, in radioulnar deviation (previously reported[7]), 23° ± 10° and 20° ± 11° in the dart-throwing motion, 13° ± 7° and 14° ± 12° in the dart-throwing-motion-inclined flexion-extension motion, and −18° ± 18° and −16° ± 12° in the opposite-dart-throwing-motion-inclined flexion-extension motion (Tables I and II). There were significant differences in the values between radioulnar deviation and the dart-throwing motion ($p < 0.0005$), between radioulnar deviation and the dart-throwing-motion-inclined flexion-extension motion ($p < 0.0005$), and between the dart-throwing-motion-inclined flexion-extension motion and the opposite-dart-throwing-motion-inclined flexion-extension motion ($p < 0.005$).

The ranges of motion of the capitate relative to the lunate and triquetrum around their own axes of rotations were 44° ± 10° and 33° ± 6°, respectively, in radioulnar deviation (as previously reported[7]), 54° ± 14° and 44° ± 12° in the dart-throwing motion, 48° ± 7° and 33° ± 8° in the dart-throwing-motion-inclined flexion-extension motion, and 41° ± 12° and 38° ± 9° in the opposite-dart-throwing-motion-inclined flexion-extension motion (Tables I and II). The values did not differ significantly among the different types of wrist motion.

Global Capitate-Based Midcarpal Motion

Regardless of the type of wrist motion, the animation of the capitate-based midcarpal motion showed that the loci of the displacement of all of the joint surfaces of the midcarpal joint

TABLE II *(continued)*

Range of Motion Around Axis of Rotation *(deg)*						
Capitate to Scaphoid	Capitate to Lunate	Capitate to Triquetrum	Scaphoid to Lunate	Triquetrum to Lunate	Scaphoid to Radius	Lunate to Radius
26	55	43	30	13	77	47
22	39	25	21	15	77	56
34	51	34	26	21	91	68
27	47	29	24	19	84	60
27	48	33	25	17	82	58
5	7	8	4	4	7	9
17	61	54	45	13	83	38
21	47	41	26	13	69	43
20	37	40	23	8	80	58
−12	23	28	16	17	61	47
18	47	38	33	15	99	70
15	44	42	33	11	124	75
5	29	24	24	16	76	53
−16	38	38	33	9	86	53
9	41	38	29	13	84.75	55
15	12	9	9	3	19	13
15	43	36	28	14	84	56
15	11	9	8	4	16	1

were located within a midcarpal ovoid space whose major axis coincided with the typical axis of rotation of the scaphoid, running from a radiopalmar to an ulnodorsal direction (Figs. 3 and 4; see Appendix for videos). A line connecting the centers of the joint surfaces of the midcarpal joint could be schematized as a letter "C" entwining the midcarpal ovoid (Figs. 3, *B*, and 5, *A*).

We also found a specific pattern of midcarpal motion for each wrist motion (Fig. 4). We previously showed that the directions and ranges of motion of the lunate and triquetrum were not significantly different from those of the scaphoid in radioulnar deviation[7]. In the dart-throwing motion, the directions of the lunate and triquetrum slightly inclined toward a wrist flexion-extension-motion plane and the ranges of motion did not change significantly compared with those in radioulnar deviation, while the direction of the scaphoid motion was not significantly different from that in radioulnar deviation but the range of scaphoid motion decreased. When the wrist was moved in a dart-throwing-motion-inclined flexion-extension-motion plane, these tendencies became more pronounced: the directions of the lunate and triquetrum inclined more, while the range of scaphoid motion decreased more. Finally, when the wrist was moved in an opposite-dart-throwing-motion-inclined flexion-extension-motion plane, the scaphoid seldom moved but the lunate and triquetrum moved along the plane of the scapholunate joint, with the range of motion not significantly changing. The lunate and triquetrum always moved separately, but the directions of the motions of the lunocapitate and triquetrohamate joints were not significantly different from each other.

In summary, as the global wrist motion changed from radioulnar deviation to the opposite-dart-throwing-motion flexion-extension motion, the range of motion of the scaphoid in the midcarpal joint gradually decreased without the direction changing significantly and the ranges of motion of the lunate and triquetrum did not significantly change but the direction gradually inclined from a dart-throwing-motion plane to an opposite-dart-throwing-motion-inclined flexion-extension-motion plane.

Motion Between the Scaphoid and Lunate and Between the Lunate and Triquetrum

The scaphoid-based animation showed that as the wrist moved from radial deviation, radial deviation/extension, or extension to ulnar deviation, ulnar deviation/flexion, or flexion, respectively, the lunate always rotated dorsally relative to the scaphoid; the relative position between the scaphoid and lunate was similar to the dorsiflexed intercalated segment insta-

bility posture (Fig. 1; see Appendix for videos).

As the global wrist motion changed from radioulnar deviation to the opposite-dart-throwing-motion-inclined flexion-extension motion, the range of rotation of the lunate relative to the scaphoid gradually increased, averaging 8° ± 6° in radioulnar deviation (as previously reported[7]), 21° ± 11° in the dart-throwing motion, 25° ± 4° in the dart-throwing-motion-inclined flexion-extension motion, and 29° ± 9° in the opposite-dart-throwing-motion-inclined flexion-extension motion (Tables I and II). There was a significant difference in the values between radioulnar deviation and the dart-throwing motion ($p < 0.001$), radioulnar deviation and the dart-throwing-motion-inclined flexion-extension motion ($p < 0.0001$), and radioulnar deviation and the opposite-dart-throwing-motion-inclined flexion-extension motion ($p < 0.0001$).

The lunotriquetral joint also moved in all types of wrist motion; however, we did not find a significant difference in the range of motion of the triquetrum relative to the lunate between radioulnar deviation, dart-throwing motion, and flexion-extension motion (Tables I and II).

Relationship Between Midcarpal and Radiocarpal Kinematics

The axes of rotation of the scaphoid and lunate relative to the radius were almost parallel to each other and passed through the neck of the capitate in all types of wrist motion. The relationship between the major axis of the midcarpal ovoid and the wrist flexion-extension axis was opposite the relationship between the axes of the radiocarpal joint and the wrist flexion-extension axis in radioulnar deviation, the relationships were similar in the dart-throwing motion, and the relationships were midway between those in radioulnar deviation and the dart-throwing motion in the flexion-extension motion.

In the axial plane, the axes of rotation of the scaphoid and lunate relative to the radius formed radially and palmarly opening angles with the wrist flexion-extension axis of −43° ± 20° and −39° ± 14°, respectively, in radioulnar deviation (as previously reported[7]); 23° ± 18° and 44° ± 27° in the dart-throwing motion; −1° ± 6° and 1° ± 3° in the dart-throwing-motion-inclined flexion-extension motion; and −2° ± 5° and −2° ± 7° in the opposite-dart-throwing-motion-inclined flexion-extension motion (Tables I and II). There were significant differences in these values between radioulnar deviation and the dart-throwing motion ($p < 0.0001$) and between the dart-throwing motion and the dart-throwing-motion-inclined flexion-extension motion ($p < 0.05$).

Discussion

We previously investigated the scaphotrapeziotrapezoid joint in cadavers both anatomically[12] and kinemati-

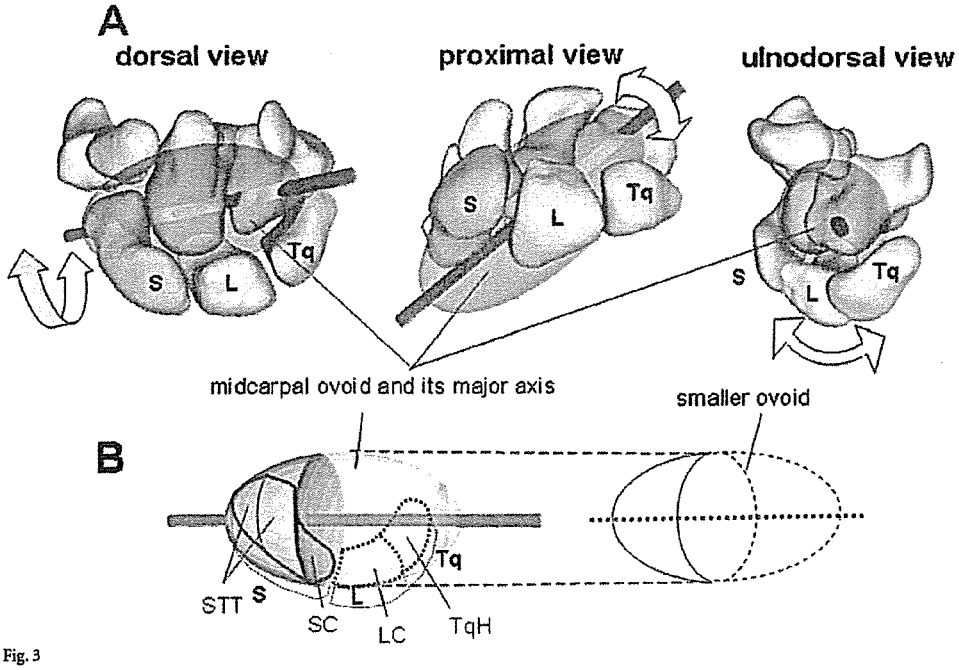

Fig. 3

A: Dorsal, proximal, and ulnodorsal views of the right carpus and a superimposed midcarpal ovoid, the major axis of which coincides with the typical axis of rotation of the scaphoid relative to the capitate. S = scaphoid, L = lunate, and Tq = triquetrum. *B:* A schematic of the dorsodistal view of the midcarpal ovoid with which the scaphotrapeziotrapezoid (STT), lunocapitate (LC), and triquetrohamate (TqH) joints come into contact. The scaphocapitate (SC) joint comes into contact with a smaller ovoid, the axis of which coincides with the major axis of the midcarpal ovoid.

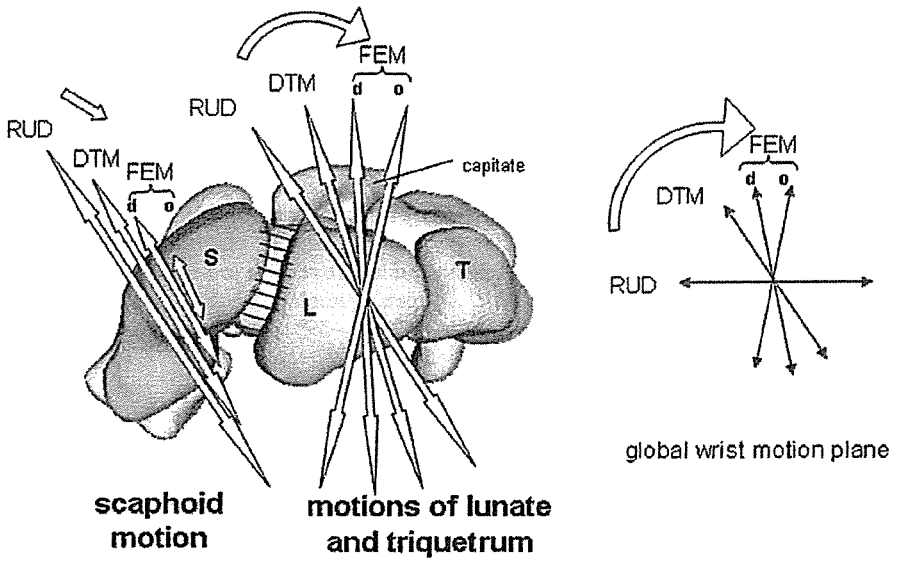

Fig. 4

Proximal view of the right carpus, showing the direction and range of motions of the scaphoid (S), lunate (L), and triquetrum (T) relative to the capitate in radioulnar deviation (RUD), the dart-throwing motion (DTM), the dart-throwing-motion-inclined flexion-extension motion (FEM) (d), and the opposite-dart-throwing-motion-inclined flexion-extension motion (o). The amount of motion is related to the length of the arrows. (See Appendix for accompanying video.)

cally[13], and those studies suggested that the scaphotrapezio-trapezoid joint has essentially a single degree of freedom, or is a uniaxial joint. The results of this current in vivo kinematic study further revealed that the range of motion of the scaphoid in the midcarpal joint gradually decreases as the global wrist motion changes from radioulnar deviation to flexion-extension motion. We noticed that the convex joint surfaces of the scaphoid articulating with the trapezium and the trapezoid can approximate an ovoid whose major axis runs from a radiopalmar to an ulnodorsal direction and coincides with the axis of rotation of the capitate relative to the scaphoid. Moreover, the concave joint surface of the scaphoid articulating with the capitate can also be a part of a smaller ovoid whose axis is the same as the major axis of the midcarpal ovoid (Fig. 3, *B*). Actually, the axis of rotation of the joint between the scaphoid and the distal carpal row is not rigid, probably because of minor mobility occurring among the trapezium, trapezoid, and capitate[14] and a lack of ligamentous constraint between the proximal part of the scaphoid and the capitate. Thus, this joint is essentially uniaxial, but it also has an adaptive mechanism that allows preservation of articular congruity of the midcarpal joint when distortional force is applied.

We have also found that the skeletal constraint of the triquetrohamate joint is relatively weak because the joint is essentially an ellipsoidal joint with two degrees of freedom, or is a biaxial joint[8]. The current study further revealed that the motion of the lunate was always similar to that of the triquetrum. Our three-dimensional analysis showed that most of the joint surfaces of the lunocapitate and triquetrohamate joints are also part of the midcarpal ovoid whose major axis runs in a radiopalmar to an ulnodorsal direction (Fig. 3, *B*). Thus, most of the joint surfaces in the midcarpal joint are contained within a midcarpal ovoid; the carpal bones might be moving within this volume, but they still have distinct motions relative to each other within it.

We consider midcarpal motion to be essentially the combined motion of three types of joint systems: (1) the uniaxial joint between the scaphoid and the distal row, the axis of which runs in a radiopalmar to an ulnodorsal direction; (2) the biaxial and ellipsoidal joint between the lunate and triquetrum and the distal row; and (3) the intercarpal joints of the proximal row, which have an adaptive mechanism that accommodates the above-mentioned two types of joint systems in the midcarpal joint. We believe that the primary motion plane in the midcarpal joint is a dart-throwing plane, which is defined by anatomical constraints of the joint between the scaphoid and the distal row; however, adaptive intercarpal motions, mainly in the scapholunate joint, and relatively weak constraints of the lunocapitate and triquetrohamate joints allow the global midcarpal joint to move in the flexion-extension or even the opposite-dart-throwing-motion-inclined flexion-extension-motion planes as well.

This study raises concerns about a self-stabilizing mechanism of the carpus under load. When the trapezium is axially loaded against the scaphoid, the scaphoid tends to rotate into flexion; this flexion moment is constrained by the extension moment experienced by the triquetrum, and stable equilibrium is achieved[15,16]. As a modification of this concept, we ad-

vocate use of an "ovoid/C" concept to explain the carpal self-stabilizing mechanism. The three-dimensional configuration of a line connecting the centers of the joint surfaces of the midcarpal joint can be schematized as a letter "C" entwining a midcarpal ovoid (Figs. 3, *B*, and 5, *A*). On the radiograph of a semisupinated wrist (Fig. 5, *B*), which is almost compatible with an axial radiograph of the ovoid, the midcarpal joint displays a C-shaped outline[7]. The ulnopalmar rotational moment of the scaphoid generated by the inclination of both the scaphotrapeziotrapezoid and the scaphocapitate joint competes and maintains balance with the radiodorsal rotational moment of the triquetrum generated by the inclination of the triquetrohamate joint (Fig. 5, *B*). Gilula and Weeks reported that three fairly smooth radiographic arcs can be drawn to define the normal carpal relationship, and disruption of any one of these lines may indicate a major carpal derangement[17]. We believe that our C-shaped outline on the radiograph of a semisupinated wrist could provide additional information about carpal derangement because this view is essentially a lateral view of the midcarpal joint.

In terms of the kinematic relationship between the midcarpal joint and the radiocarpal joint, the question arises of how the oblique midcarpal motion accommodates itself to radiocarpal motion. It is well known that, during radioulnar deviation, the three proximal carpal bones move synergistically relative to the radius from a flexed and radially deviated position in wrist radial deviation to an extended and ulnarly deviated position in wrist ulnar deviation[5,18-20]. This finding is consistent with our observation that the axes of rotation of the proximal row relative to the radius run in a radiodorsal to an ulnopalmar direction. The relationship between the primary axes of the midcarpal joint and the radiocarpal joint during radioulnar deviation is reciprocal, effectively canceling rotation in the flexion-extension plane of the hand on the forearm. During the dart-throwing motion, the axes of the two joints are similar and synergistic with each other, which may explain why the range of wrist motion achieved in this plane is greater than that achieved in radioulnar deviation and why the dart-throwing plane is the usual

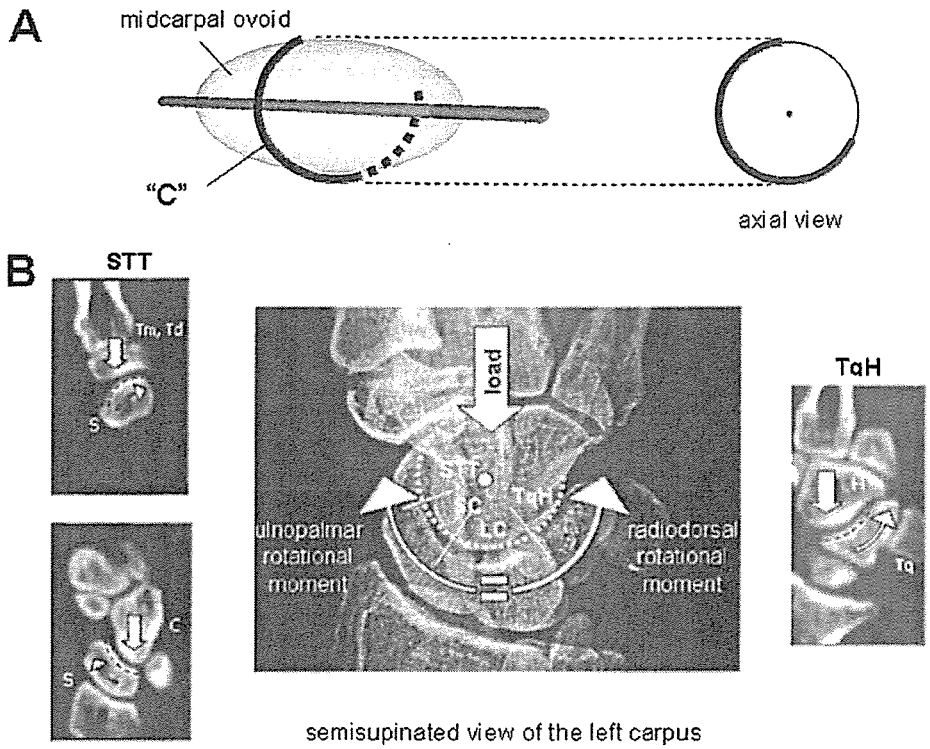

Fig. 5

The "ovoid/C" concept. *A:* The three-dimensional configuration of a line connecting the centers of the joint surfaces of the midcarpal joint can be schematized as a letter "C" entwining a midcarpal ovoid. The "C" clearly appears to form a three-quarter circle in the axial view of the ovoid. *B:* Semisupinated radiograph of the left carpus, which is compatible with an axial view of the ovoid of the right carpus, and the tomograms at the level of the scaphotrapeziotrapezoid (STT), scaphocapitate (SC), and triquetrohamate (TqH) joints. In this plane, the midcarpal joint displays a C-shaped outline, and the ulnopalmar rotational moment of the scaphoid generated by the inclination of the scaphotrapeziotrapezoid and scaphocapitate joints maintains balance with the radiodorsal rotational moment of the triquetrum generated by the inclination of the triquetrohamate joint.

plane of utilization of the wrist[21]. During flexion-extension motion, the axis of the radiocarpal joint is almost the same as the wrist flexion-extension axis and the axis of the midcarpal joint is oblique, findings that are consistent with the fact that, normally, extension of the wrist is associated with radial deviation and flexion is associated with ulnar deviation[18].

Our current kinematic technique has some limitations, the greatest of which is that the study was based on static three-dimensional views of the carpus in the limited number of wrist positions examined. The static measurement does not include any inertial or functional effects that might occur during normal wrist motion. The angles of the axis of rotation would not be fixed angles for the entire range of motion; they would have varied if we had used more increments of motion. It would be reasonable to perform dynamic studies to supplement this study. We tried to establish the wrist dart-throwing motion as an oblique wrist motion relative to the sagittal plane, but there is no consensus about what constitutes the true plane of the wrist dart-throwing motion[22]. However, the technique that we used in this study allowed us to obtain new information on in vivo three-dimensional midcarpal kinematics without subjecting the volunteers to radioactive exposure. Our findings suggest that the proximal carpal row with all its related joints has a unique mechanism that contributes to both the stability and the mobility of the wrist. Hopefully, this new information on the ovoid/C-shape perspective of the anatomy and the kinematics of the midcarpal joint will assist clinicians in obtaining a better understanding of the wrist joint and some of its disorders.

Appendix

(eA) Videos of the midcarpal motions (as supplements to Figures 1 and 4) are available on our web site at jbjs.org (go to the article citation and click on "Supplementary Material"). ■

Hisao Moritomo, MD
Tsuyoshi Murase, MD
Akira Goto, MD
Kunihiro Oka, MD
Kazuomi Sugamoto, MD
Hideki Yoshikawa, MD, PhD
Department of Orthopaedic Surgery, Osaka University, 2-2 Yamadaoka, Suita-shi, Osaka 565-0871, Japan. E-mail address for H. Moritomo: moritomo@ort.med.osaka-u.ac.jp

In support of their research for or preparation of this manuscript, one or more of the authors received Grants-in-Aid for Scientific Research, the Ministry of Education, Science and Culture in Japan, and Grant of Japan Orthopaedics and Traumatology Foundation, Inc. (No. 0146). None of the authors received payments or other benefits or a commitment or agreement to provide such benefits from a commercial entity. No commercial entity paid or directed, or agreed to pay or direct, any benefits to any research fund, foundation, educational institution, or other charitable or nonprofit organization with which the authors are affiliated or associated.

doi:10.2106/JBJS.D.02885

References

1. Kobayashi M, Berger RA, Linscheid RL, An KN. Intercarpal kinematics during wrist motion. Hand Clin. 1997;13:143-9.

2. de Lange A, Kauer JM, Huiskes R. Kinematic behavior of the human wrist joint: a roentgen-stereophotogrammetric analysis. J Orthop Res. 1985;3:56-64.

3. Ruby LK, Cooney WP 3rd, An KN, Linscheid RL, Chao EY. Relative motion of selected carpal bones: a kinematic analysis of the normal wrist. J Hand Surg [Am]. 1988;13:1-10.

4. Savelberg HH, Otten JD, Kooloos JG, Huiskes R, Kauer JM. Carpal bone kinematics and ligament lengthening studied for the full range of joint movement. J Biomech. 1993;26:1389-402.

5. Kauer JM. The interdependence of carpal articulation chains. Acta Anat (Basel). 1974;88:481-501.

6. Seradge H, Sterbank PT, Seradge E, Owens W. Segmental motion of the proximal carpal row: their global effect on the wrist motion. J Hand Surg [Am]. 1990;15:236-9.

7. Moritomo H, Murase T, Goto A, Oka K, Sugamoto K, Yoshikawa H. Capitate-based kinematics of the midcarpal joint during wrist radioulnar deviation: an in vivo three-dimensional motion analysis. J Hand Surg [Am]. 2004;29:668-75.

8. Moritomo H, Goto A, Sato Y, Sugamoto K, Murase T, Yoshikawa H. The triquetrum-hamate joint: an anatomic and in vivo three-dimensional kinematic study. J Hand Surg [Am]. 2003;28:797-805.

9. Goto A, Moritomo H, Murase T, Oka K, Sugamoto K, Arimura T, Nakajima Y, Yamazaki T, Sato Y, Tamura S, Yoshikawa H, Ochi T. In vivo elbow biomechanical analysis during flexion: three-dimensional motion analysis using magnetic resonance imaging. J Shoulder Elbow Surg. 2004;13:441-7.

10. Patterson RM, Nicodemus CL, Viegas SF, Elder KW, Rosenblatt J. High-speed, three-dimensional kinematic analysis of the normal wrist. J Hand Surg [Am]. 1998;23:446-53.

11. Panjabi MM, Krag MH, Goel VK. A technique for measurement and description of three-dimensional six degree-of-freedom motion of a body joint with an application to the human spine. J Biomech. 1981;14:447-60.

12. Moritomo H, Viegas SF, Nakamura K, Dasilva MF, Patterson RM. The scaphotrapezio-trapezoidal joint. Part 1: an anatomic and radiographic study. J Hand Surg [Am]. 2000;25:899-910.

13. Moritomo H, Viegas SF, Elder K, Nakamura K, Dasilva MF, Patterson RM. The scaphotrapezio-trapezoidal joint. Part 2: a kinematic study. J Hand Surg [Am]. 2000;25:911-20.

14. Sonenblum SE, Crisco JJ, Kang L, Akelman E. In vivo motion of the scaphotrapezio-trapezoidal (STT) joint. J Biomech. 2004;37:645-52.

15. Kobayashi M, Garcia-Elias M, Nagy L, Ritt MJ, An KN, Cooney WP, Linscheid RL. Axial loading induces rotation of the proximal carpal row bones around unique screw-displacement axes. J Biomech. 1997;30:1165-7.

16. Garcia-Elias M, Lluch A. Partial excision of scaphoid: is it ever indicated? Hand Clin. 2001;17:687-95, x.

17. Gilula LA, Weeks PM. Post-traumatic ligamentous instabilities of the wrist. Radiology. 1978;129:641-51.

18. Fisk G. Biomechanics of the wrist joint. In: Tubiana R, editor. The hand. Philadelphia: WB Saunders; 1981. p 136-41.

19. Horii E, Garcia-Elias M, An KN, Bishop AT, Cooney WP, Linscheid RL, Chao EY. A kinematic study of luno-triquetral dissociations. J Hand Surg [Am]. 1991; 16:355-62.

20. Garcia-Elias M. Kinetic analysis of carpal stability during grip. Hand Clin. 1997;13:151-8.

21. Saffer P, Semaan I. The study of the biomechanics of wrist movements in an oblique plane—a preliminary report. In: An KN, Garcia-Elias M, Cooney WP 3rd, Schuind F, editors. Advances in the biomechanics of the hand and wrist. New York: Plenum Press; 1994. p 305-11.

22. Werner FW, Green JK, Short WH, Masaoka S. Scaphoid and lunate motion during a wrist dart throw motion. J Hand Surg [Am]. 2004;29:418-22.

Modulation of Peritendinous Adhesion Formation by Alginate Solution in a Rabbit Flexor Tendon Model

Jiro Namba,[1] Kozo Shimada,[2] Masanobu Saito,[3] Tsuyoshi Murase,[4] Hideaki Yamada,[5] Hideki Yoshikawa[4]

[1] Department of Orthopaedic Surgery, Minoh City Hospital, 5-7-1, Kayano, Minoh, Osaka 562-0014, Japan

[2] Department of Orthopaedic Surgery, Rinku General Medical Center, Izumisano Municipal Hospital, 2-23, Rinku Orai-kita, Izumisano, Osaka 598-0048, Japan

[3] Department of Orthopaedic Surgery, Osaka-minami Medical Center, 2-1, Kidohigashi, Kawachinagano, Osaka 586-0008, Japan

[4] Department of Orthopaedic Surgery, Osaka University Graduate School of Medicine, 2-2, Yamada-oka, Suita, Osaka 565-0871, Japan

[5] Medical Research Group, Kuraray Medical Company, Ltd., 1621, Sakazu, Kurashiki, Okayama 710-8622, Japan

Received 5 March 2005; revised 3 December 2005; accepted 27 February 2006
Published online 9 June 2006 in Wiley InterScience (www.interscience.wiley.com). DOI: 10.1002/jbm.b.30594

Abstract: To examine the antiadhesive effect of an alginate solution following tendon surgery, unilateral subtotal laceration of the flexor digitorum communis tendon was created in one hind limb while the other side was left intact in 32 Japanese white rabbits. The lesion was coated with alginate solution in 16 animals and not coated in the other 16. Degree of adhesion formation was assessed histologically and biomechanically by measuring the flexion angle of the first toe when the flexor digitorum tendon was pulled with a specified force at 4 weeks postoperatively. When compared with the control group, the alginate-treated group demonstrated significantly greater toe flexion, with less scar tissue formation at the repair site. Histologically, complete tendon healing with longitudinal remodeling of collagen fibers was observed in the alginate-treated group, while a random pattern of fibers was observed in the control group. Reduction in adhesion formation using alginate solution represents a novel strategy for the management of tendon injury and repair in the clinical setting. © 2006 Wiley Periodicals, Inc. J Biomed Mater Res Part B: Appl Biomater 80B: 273–279, 2007

Keywords: alginate; tendon; adhesion; polysaccharide; tendon repair

INTRODUCTION

Peritendinous adhesion is a major problem following tendon surgery. Adhesions interfere with tendon gliding and restrict tendon excursion, thereby causing poor functional results after tendon repair. Until recently, many investigators considered the tendon to have the ability to heal itself (intrinsic theory) and believed that the extrinsic mechanism, which is an inflammatory response to injury, is not essential to the healing process. A number of methods, most of which use mechanical barriers, including synthetic materials,[1–3] around the repair site, have been applied in order to physically block scar tissue intrusion, but no satisfactory approach has been established to date.

Debate concerning tendon repair has continued and it is now generally accepted that tendons heal by a combination of both intrinsic and extrinsic mechanisms,[4,5] although there seems to be an imbalance between the two mechanisms during the initial phase of tendon healing.[6] During this phase, the extrinsic mechanism predominates over the intrinsic mechanism, the onset of which is delayed. We hypothesized that the best approach to reduce peritendinous adhesion is not to prevent extrinsic mechanisms completely, but to modulate the behavior of extrinsic-derived cells. That is to say, antiadhesive materials should be selectively permeable, allowing permeation of low-molecular-weight nutritional substances, which are essential for the intrinsic mechanism, but not entities at the cell-size level such as fibroblasts and leukocytes that migrate from the extrinsic field.

One such candidate is alginate, an intercellular polysaccharide known to be widely distributed in brown seaweed. Alginate is utilized in immobilizing living cells because of its easy gelation, good biocompatibility, and low toxicity.[7] In

Correspondence to: J. Namba (e-mail: yonamba@ybb.ne.jp or hospital@maple.city.minoh.lg.jp)

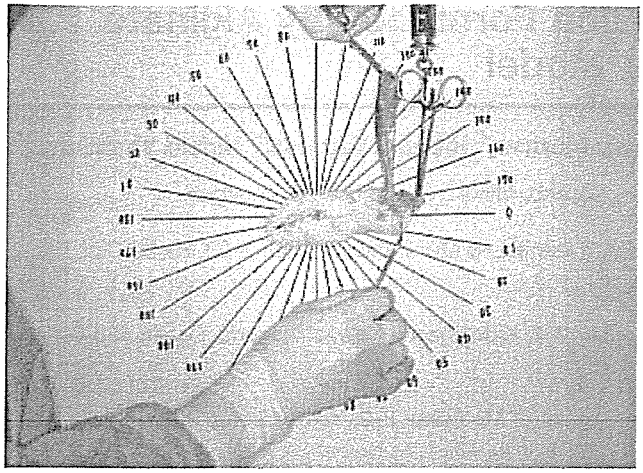

Figure 1. The method of mechanical evaluation. The limb was placed in a vertical position with its proximal tibia and calcaneus immobilized by a clamp. The leg was observed from the medial side in front of a white screen bearing radial lines representing a protractor. The first metatarsophalangeal joint was positioned at the center of the protractor. The flexion angle of the first toe was measured at the rest position and when pulled with a 400-g force (measured with a spring-type scale). The flexion range of motion was determined as the difference between the rest position and the flexed position.

allo- and xenogeneic islet transplantation, the best results have been obtained with alginate microcapsules; success in this procedure was attained by enclosing grafts in a selectively permeable alginate membrane.[8] The membrane only allows the permeation of smaller molecules, such as oxygen, glucose and insulin, preventing the penetration of immunocytes and larger immune molecules.[8] We hypothesized that the same cell immobilization effect would occur in the application of alginate to injured tendon. The present study investigated whether a beneficial antiadhesive effect could be obtained using alginate solution on rabbit tendon injury.

MATERIALS AND METHODS

Experimental Animals

Thirty-two Japanese white rabbits weighing around 3000 g were used. All rabbits were free of disease, and each experimental procedure was approved by the Committee on the Use and Care of Animals of Kuraray Co..

Preparation of Alginate Solution

Sodium alginate powder used in the experiment was derived from *Lassonia nigrescens* (Kimitsu Chemical Industries, Japan). This substance had the following characteristics as reported by the manufacturer: M/G (β-D-mannuronic acid/α-L-guluronic acid) ratio, 1.3; weight-average molecular weight, $M_w/10^4 = 54$; and polydispersity index, $M_w/M_n = 5.43$. It had a purity of at least 99% and was sterile, but was not specified as being pyrogen-free. However, the Limulus amebocyte lysate testing showed that the alginate's endotoxin concentration was less than 10 EU/g. When typical concentrations of sodium alginate solution and $CaCl_2$ solution are used in cell encapsulation, sodium alginate rapidly forms a hard gel that cannot be applied as a coatable or injectable tendon adhesion barrier gel. To overcome this phenomenon, very high concentrations of sodium alginate were utilized without the crosslinking method. The alginate solution was first adjusted to a concentration of 10% (by weight). Autoclave sterilization at 121°C for 20 min was then done to depolymerize the alginate solution and to reduce the molecular weight to $2.4-4.0 \times 10^5$ M_w (as measured by high-speed liquid chromatography, Waters Alliance, Waters, Japan). Final processed alginate solution remained 10% concentrated and was adequately viscous for injection and coating.

Surgical Procedure

Full-thickness lacerations were used in a preliminary study; however, when this was performed, tendons were ruptured or

TABLE I. Flexion Angle Percentage[a]

Animal Number	Flexion Angle (%)
Alginate-treated group	
1	87.5
2	87.5
3	81.8
4	100
5	100
6	87.5
7	70
8	66.7
9	81.8
10	66.7
11	37.5
12	100
13	87.5
14	100
15	88.9
16	60
Control	
17	70
18	70
19	63.6
20	77.8
21	50
22	80
23	44.4
24	55.6
25	75
26	54.5
27	77.8
28	63.6
29	28.6
30	100
31	50
32	70

[a] Calculated by dividing operated side δ angle by nonoperated side δ angle (i.e. the difference between resting toe flexion angle and toe flexion angle with force applied).

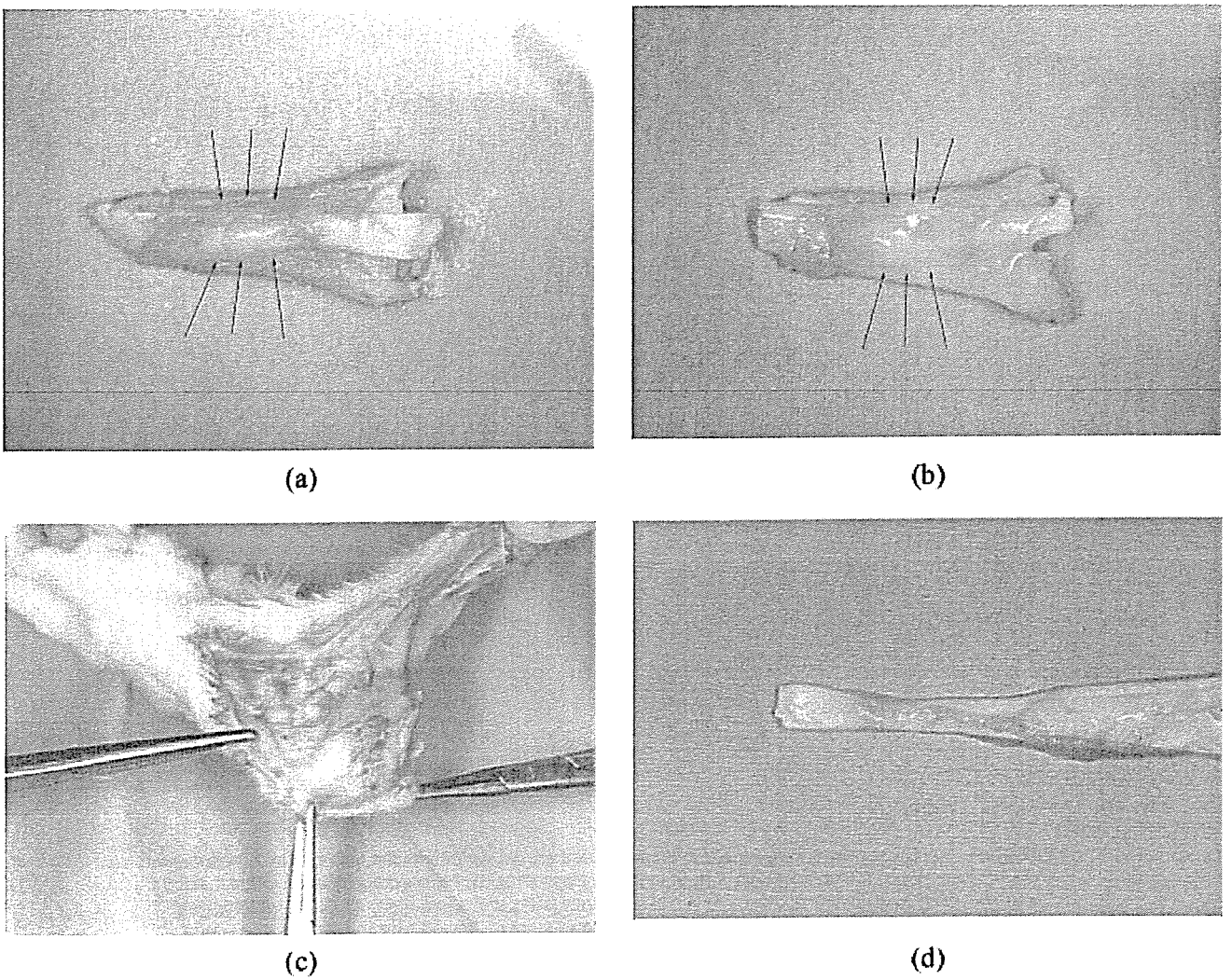

Figure 2. (a) Appearance of the lesion site in the control group. Degree of scar formation at the repaired tendon was greater (arrows) in the control group than in the alginate-treated group. (b) Macroscopic appearance of the lesion site in the alginate-treated group. In the alginate-treated group, the repaired tendon was surrounded by a transparent membrane (arrows). (c) Macroscopic appearance of the lesion site. A yellowish gel thought to be undissolved alginate was seen in the intact part of the sheath at week 4. (d) Macroscopic appearance of the lacerated tendon in the alginate-treated group. Repair of the tendon appeared complete.

severe contractures occurred in some animals and stable adhesion was not possible in this rabbit model. We therefore used partial lacerations in the present model to avoid the variability inherent in full-thickness lacerations.[9-12] Surgical procedure was based on the model used in an earlier study.[9]

Rabbits were anesthetized with an intravenous infusion of ketamine hydrochloride (0.5 mg/kg). After preparation of the hind limb, the skin was incised and the tendon sheath of the flexor digitorum communis muscle was exposed just above the ankle. The sheath was opened transversely and the tendon isolated. The toes were then maximally flexed and the intrasynovial part of the tendon was drawn into the wound. Using a scalpel blade, the tendon on the medial side was divided transversely as distally as possible, with the resulting laceration affecting ~50% of the volume of the structure. In 16 animals, the site of the lesion was coated with 1.0 g (by weight) of alginate paste (10% solution) (alginate group), while the remaining 16 received no such coating (control group). After surgery, the toes were placed back into the neutral position, allowing the injured portion of the tendon to slide distally to lie within an undisturbed part of the sheath. The excised sheath was not repaired and the skin was closed with 3-0 nylon. Postoperative immobilization was not applied.

Mechanical Evaluation

At 4 weeks postoperatively, the 16 animals in each group were killed by anesthetic overdose. Both legs were disartic-